Journal of Colloid and Interface Science 678 (2025) 400–409

Contents lists available at ScienceDirect

Journal of Colloid And Interface Science

journal homepage: www.elsevier.com/locate/jcis

Regular Article

How bulk liquid viscosity shapes capillary suspensions ☆

Christoph Haessig [a], Jasper Landman [a], Elke Scholten [a,*], Ahmed Jarray [a,b,*]

[a] Physics and Physical Chemistry of Foods, Wageningen University, PO Box 17, 6700 AA Wageningen, the Netherlands
[b] Multi Scale Mechanics (MSM), MESA+ Institute for Nanotechnology, University of Twente, P.O. Box 217, 7500 AE Enschede, the Netherlands

GRAPHICAL ABSTRACT

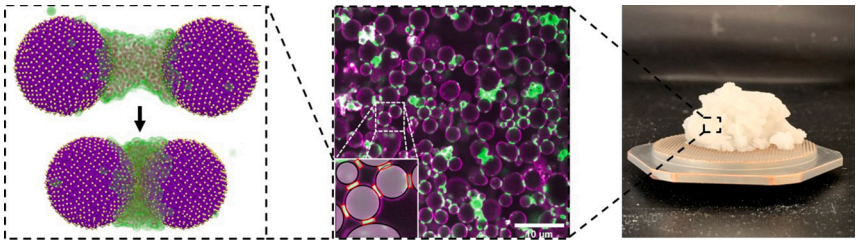

ARTICLE INFO

Keywords:
Capillary suspensions
Capillary bridges
Gel
Viscosity
Colloidal suspensions

ABSTRACT

Hypothesis: Capillary suspensions offer a new approach to generate novel materials. They are ternary liquid-liquid-solid systems characterized by particles connected by liquid bridges of one fluid suspended in a second immiscible bulk fluid. The viscosity of the bulk liquid can be modulated to customize the structure and rheological properties of capillary suspensions.

Experiments and simulations: Using experiments and numerical simulations, we investigated capillary suspensions in the pendular state, using silica particles and water as a bridging liquid. To modulate the viscosity of the bulk fluid, we use different ratios of either dodecane and diisononyl phthalate, or silicone oils with varying chain lengths as bulk liquids. The rheological behavior was characterized using the maximum storage and loss moduli and the yielding behavior. This was related to structural changes of the systems, which was visualized using confocal laser scanning microscopy. In addition, we used Molecular Dynamics (MD) simulations to gain more insights into the behavior of two particles connected by a liquid bridge for various bulk liquids.

Findings: Experiments show that higher bulk liquid viscosity reduces strength, yield stress, and yield strain in capillary suspensions, which is partly attributed to a reduced inter-connectivity of the percolating network. This is caused by the breakup of liquid bridges occurring at shorter distances in the presence of highly viscous bulk liquids, as indicated by numerical simulations.

☆ Electronic Supplementary Information (ESI) available.

* Corresponding authors.
E-mail addresses: christoph.haessig@gmail.com (C. Haessig), jasper.landman@wur.nl (J. Landman), elke.scholten@wur.nl (E. Scholten), ahmed.jarray@wur.nl (A. Jarray).

https://doi.org/10.1016/j.jcis.2024.09.021
Received 8 April 2024; Received in revised form 30 August 2024; Accepted 2 September 2024
Available online 5 September 2024

1. Introduction

Capillary suspensions are ternary liquid-liquid-solid systems formed by the addition of small amounts of an immiscible secondary liquid to particle suspensions. The formation of secondary liquid bridges between the suspended particles induces the formation of a space-spanning network and consequently drastically changes the rheological behavior [1]. This phenomenon makes capillary suspensions suitable for the production of novel materials, such as highly porous materials [2–4], stimuli-responsive materials [5], conductive pastes for solar cells [6], crack-free films [7], slurries for battery electrodes [8], 3D printing pastes [9,10], and novel food products [11,12].

Depending on the wetting ability of the secondary liquid, two different states can be distinguished; The pendular state is formed when the secondary liquid preferably wets the particles, and the capillary state is formed when the secondary liquid is preferably non-wetting [13]. In the pendular state, particles are connected by concave liquid bridges, whereas in the capillary state, particles form clusters around secondary fluid droplets [14]. In both cases, clusters are formed that serve as building blocks for network formation, that drastically increases the stability and gel strength [15,16]. As the capillary force arising from the liquid bridge formation often dominates over other colloidal forces, the changes in properties are substantial [17].

Considerable attention has been directed towards understanding the variables affecting the structure and mechanical properties of capillary suspensions [15,18–20]. The forces exerted on the network of capillary suspensions depend on the particle radius r, the interfacial tension Γ between the bulk and secondary liquid, and the wetting behavior of both liquids characterized by the three-phase contact angle θ [19]. Additionally, the number and volume of pendular bridges or secondary liquid droplets are critical determinants of strength and structure in the pendular and capillary states, respectively [20]. In the pendular state, the capillary bridge force can be calculated by assuming a specific bridge shape or by solving the Young-Laplace equation [20]. A simplified expression for the capillary force in the pendular state is given by

$$F_c = 2\pi r \Gamma \cos(\theta) \tag{1}$$

assuming that the particles are in close contact and that the size of the pendular bridge is small relative to that of the particles [21,22]. Furthermore, the macroscopic gel strength of capillary suspensions can be derived from the capillary force between two particles and the structural properties of the network. The yield stress is related to the capillary bridge force, assuming equally-sized particles in direct contact, by [15,23–25]

$$\sigma_y = f(\phi,\ N)\frac{F_c}{r^2} = f(\phi,\ N)\, g(V)\frac{F_c}{r}, \tag{2}$$

with $f(\phi,\ N)$ being a function of the particle volume fraction and the number of capillary bridges per unit volume [13,26] and $g(V)$ a function of the bridge volume. The number and volume of the capillary bridges depend on the secondary liquid volume fraction but also on the mixing conditions during the sample preparation, as capillary suspensions are not in thermodynamic equilibrium [27].

The secondary liquid must be dispersed into small droplets for network formation, underlining the importance of droplet breakup conditions during capillary suspension preparation. The influence of the mixing conditions on the structure and rheological properties of capillary suspensions has been recently investigated by Bossler at al. [20], who showed that more homogeneous and stronger networks are achieved through enhanced droplet breakup. Grace [28] showed that the smallest droplets are obtained when the viscosity ratio between the secondary (bridging) and bulk liquid, $\eta_{\text{sec. liquid}}/\eta_{\text{bulk liquid}}$, in capillary suspension ranges from 0.1 to 1.

Although the effect of viscosity on droplet break-up has been previously discussed, the influence of the viscosity ratio in the context of capillary suspensions has been studied only by Hoffmann et al. [12], specifically for corn starch and cocoa particle suspensions. They varied the viscosity of the secondary (bridging) liquid but found no impact of the viscosity ratio on the yield stress in both capillary and pendular state suspensions. This limited effect was attributed to diffusion-driven bridge formation. Other studies have focused on the properties of the secondary liquid. For instance, Yang et al. [29] investigated capillary suspensions where sodium alginate (SA) was added to the secondary liquid. They found that SA significantly enhances the gel strength of the suspensions due to its well-known ability to form hydrogen bonds. Das et al. [5] hypothesized that capillary suspensions with low-viscosity, flowable liquid bridges exhibit lower yield stress, while those with gelled and highly viscous bridges exhibit higher yield stress. Ahuja and Gamonpilas [30] demonstrated that transitioning the secondary liquid from a low-viscosity fluid to a gel-like material leads to an increase in the storage modulus of capillary suspensions. Furthermore, the available research on the effect of viscosity on liquid bridges breakage were conducted with air as the continuous phase fluid [31–33]. Shi et al. [34] studied the dynamic stretching of a liquid bridge between two glass plates across liquids of varying viscosities, demonstrating that viscous forces significantly affect contact angle hysteresis. Li et al. [35] noted that as the volume of the liquid bridge expands, the viscous force increasingly impacts the critical rupture distance. To the best of our knowledge, no study has investigated the effect of the bulk liquid viscosity on the structure and resulting rheological behavior of capillary suspensions. Furthermore, the role of the micro-structural dynamics of the liquid bridges present between the particles surrounded by a viscous liquid is still unexplored.

To address this knowledge gap, we explore how the viscosity of the bulk liquid affects the structure and rheological behavior of pendular state capillary suspensions. We established connections between macroscopic changes in behavior, alterations in the network structure, and modifications in the behavior of individual secondary liquid bridges. First, we discuss the impact of secondary liquid addition on the rheological behavior of suspensions. Subsequently, we analyze the effect of bulk liquid viscosity on the gel strength and yielding behavior of pendular state capillary suspensions. This was further related to changes in the network structure. Finally, numerical simulations were employed to explain the observed experimental decrease of the average number of bridges per particle with increasing bulk liquid viscosity.

2. Materials and methods

2.1. Materials

Powders of solid spherical silica particles with sizes of ~5 and ~10 μm were purchased from US Research Nanomaterials (Houston, U.S.). The particles were used as provided. Dodecane (n-Dodecane, 99%) was purchased from Thermo scientific (Waltham, U.S.). Diisononyl phthalate (DINP)(technical grade) was purchased from Sigma-Aldrich (St. Louis, U.S.). Silicone oils with kinetic viscosities of 5 cSt and 1000 cSt at 25 °C were purchased from Sigma-Aldrich (St. Louis, U.S.). Acetone (AR-grade) was obtained from Actu-All Chemicals (Oss, The Netherlands). The fluorescent dyes fluorescein amine and Rhodamine B were obtained from Sigma-Aldrich (St. Louis, U.S.). Ultrapure water (MilliQ Purelab Ultra, Germany) was used for all experiments.

2.2. Experimental methods

2.2.1. Sample preparation

Bulk liquid preparation Bulk liquids with varying viscosities were prepared by mixing two bulk liquid components at room temperature. The first bulk liquid system consisted of dodecane and DINP and was prepared at dodecane volume concentrations of 0, 2, 5, 10, 15, 25, 30, 40, 50, 75, and 100% (v/v). The second bulk liquid system was prepared by mixing two silicone oils (5 cSt and 1000 cSt at 25 °C) at 1000 cSt silicone oil volume concentrations of 0, 5, 15, 25, 35, 45, 50, 55, 65, 75, 80, and 100% (v/v).

Preparation of capillary suspensions The particle suspensions were prepared by first adding silica particles to the bulk liquid while being stirred at 400 rpm with an overhead stirrer (RW 20D, IKA-Werke, Staufen, Germany), equipped with a propellor mixer (28 mm radius). The silica particles were initially dry and sealed to prevent moisture adsorption and were used directly for capillary suspension preparation, minimizing exposure to air. The suspension was further mixed at 1400 rpm for 5 minutes to obtain a homogeneous mixture. Then, capillary suspensions were obtained by adding the secondary liquid (i.e., water) dropwise to the particle suspensions while stirring at 1400 rpm. After water addition, the samples were mixed at 1400 rpm for 30 minutes. The capillary suspensions with silicone oil bulk liquids were additionally homogenized with a rotor-stator-homogenizer (T25 digital Ultra Turrax, IKA-Werke, Staufen, Germany) at 12000 rpm for 5 minutes. The same volume percentages were used throughout the study; with 20% (v/v) of silica particles, 1.5% (v/v) of water and 78.5% (v/v) of bulk liquid.

2.2.2. Rheological measurements

Rotational rheology The viscosity of the different bulk liquids was measured using a stress-controlled MCR 502 rheometer (Anton Paar GmbH, Graz, Austria) equipped with a Peltier element and a concentric cylinder geometry (probe: CC17/Ti–3953; cup: C-CC17/Ti– 50622). The shear rate was increased from 1 to 100 s^{-1} in a period of 17 minutes. The bulk liquid viscosity was obtained through regression of the viscosity curve using the RheoCompass software (Anton Paar GmbH, Graz, Austria) at room temperature.

Oscillatory rheology To quantify the macroscopic gel properties of the particle and capillary suspensions prepared with different bulk liquid viscosities, amplitude sweeps were performed. The measurements were performed with a stress-controlled MCR 502 rheometer (Anton Paar GmbH, Graz, Austria) equipped with a Peltier element and profiled 50 mm plate-plate geometry to avoid wall slip (upper plate model PP50/P2/SS-69022; lower plate inset PP50/SS). All samples were measured at a gap size of 1 mm, except for those with bulk liquid compositions equal or greater than 40% dodecane. The surface of the plate-plate geometry was dried before each measurement with a compressed air gun and an absorbent sheet. The obtained gel samples with dodecane contents equal or above 40% were too strong and were measured at a variable gap height corresponding to a normal force of 40 N. After preshearing the sample at a shear strain of 0.01% and a frequency of 1 Hz for 10 minutes, the shear strain γ was logarithmically increased from 0.001% to 1000% at a constant angular frequency ω of 1.6 Hz. Both storage modulus, G', and loss modulus, G'', were recorded in a time frame of 25 minutes.

The maximum storage modulus (G') was determined as the average within the linear viscoelastic range, up to the point where G' decreased by 3% from its initial value [36]. The maximum loss modulus was acquired by calculating the maximum of the loss modulus-strain function. The first yield stress was determined using the RheoCompass software by a linear weighting of the shear stress at the onset of the amplitude sweeps curve, right before the rapid decline of the shear stress [37]. The corresponding strain was defined as first yield strain.

The particle suspensions and dodecane-DINP continuous capillary suspensions were measured within 5 hours, and the silicone oil-continuous capillary suspensions were measured directly after preparation. The measurements were performed in triplicate. The temperature was constant at 20 °C during all measurements. To confirm the absence of slippage, we conducted measurements of the storage modulus with DINP and dodecanes as bulk liquids for different gap sizes between the plates. The results, which demonstrated a consistent match, are displayed in Figure S1 in the supplementary information (SI) appendix.

2.2.3. Confocal laser scanning microscopy (CLSM)

CLSM-images were taken to gain insights into the effect of the bulk liquid viscosity on the network structures of the capillary suspensions. The silica particles were stained using a 0.005% (w/w) Rhodamine B in acetone solution. 50 g of silica particles were mixed with 60 ml of the Rhodamine B solution by stirring twice for a minute with a break of 10 minutes between the stirring intervals. Acetone was then allowed to evaporate. The dyed secondary bridging liquid was prepared by mixing 0.5 g of fluorescein amine with 200 ml of water. The particle and capillary suspensions were prepared by dispersing the stained silica particles in the bulk liquid using a rotor-stator-homogenizer (T25 digital Ultra Turrax, IKA-Werke, Staufen Germany) at 12000 rpm for 5 minutes. Afterwards, the particle and capillary suspensions were prepared by adding the dyed secondary bridging liquid (water). A small portion of the dyed capillary suspension sample was gently placed between a microscope slide and cover glass to minimize any additional shear that might influence the microstructure. Additionally, a spacer was used to maintain a consistent gap and prevent compression. To ensure that the addition of dye did not alter the network structure, we measured the rheological properties of the dyed samples and compared them to the non-dyed samples of dodecane and DINP, as shown in Figure S2 of the SI appendix.

The images were taken using a ReScan Confocal unit (Confocal.nl, Amsterdam, The Netherlands) connected to a PCM2000 microscope (Nikon Europe BV, Amsterdam, The Netherlands). The microscope was equipped with a 60x/1.2W objective (Nikon Europe BV, Amsterdam, The Netherlands). Lasers with wavelengths of 561 nm and 488 nm were used to excite the Rhodamine B and fluorescein to visualize the silica particles and the secondary liquid bridges, respectively. To ensure the confocal images accurately represent the suspension's structure, duplicate samples were prepared and imaged using CLSM.

The CLSM Images were post-processed using ImageJ (version 1.52) [38]. The 16-bit images were converted into RGB images, and the brightness and contrast were adjusted to make all components visible. To obtain information about the structural organization of the capillary suspensions with increasing bulk liquid viscosity, the number of nearest neighbors was calculated based on the obtained CLSM images. The average number of capillary bridges per particle was computed as the ratio between the number of capillary bridges divided by half of the number of silica particles in the image. The number of particles and capillary bridges was counted manually in three images per sample, where a spatial annotation counting approach was used, ensuring no miscounts by marking particles and bridges in each image. When particles appeared as part of larger continuous blobs of the secondary liquid, each connection to the blob was counted as an individual bridge. We provide an example of the counting approach in Figure S3 of the SI Appendix. The process was conducted independently by two researchers several times to verify the consistency of the results.

2.3. Molecular dynamics simulations

Molecular Dynamics (MD) simulations were utilized to study the effect of viscosity on the dynamics of liquid bridges between two particles. Despite the scale difference between the nanoscale simulations and our microscale experiments, MD simulations can provide fundamental insights into the behavior and interaction of molecules of the different components of capillary suspensions, extrapolating this knowledge to larger scales. Previous studies have demonstrated the efficiency of using MD simulations to interpret microscale behaviors by providing a detailed understanding of the nanoscale interactions and dynamics [39–41].

Using the large-scale atomic/molecular massively parallel simulator (LAMMPS) package [42], All-atom (MD) simulations were carried out to investigate the water liquid droplet breaking within the bulk liquids. The atomistic system was subjected to the COMPASS forcefield [43], where the van der Waals interactions are accounted for by 12-6 Lennard-Jones and Coulomb electric potentials. The Particle Particle Particle Mesh (PPPM) technique computes the long-range Coulombic interactions with an accuracy of 10^{-4} kcal/mol, whereas the van der

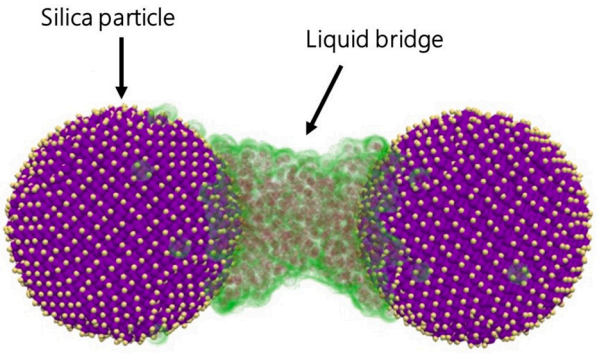

Fig. 1. Atomistic model of two nanoparticles in contact with a water liquid bridge, taken at timestep $t = 20$ ps. Silica particles are colored in magenta and the bulk liquid is transparent (For interpretation of the colors in the figure(s), the reader is referred to the web version of this article).

Waals interactions were smoothly truncated at a distance of 12.5 Å. With a time step of 1 fs, the Newtonian motion equations for each atom were solved using the Velocity-Verlet algorithm.

The atomistic model consists of two spherical silica particles of 4.5 nm diameter. The silica model encompasses the interacting atoms located at the hydroxilated silicon dioxide interface, thereby ensuring similar intermolecular interactions [44,45]. The particles are in contact with a bridge of water molecules, and placed in a simulation cell of size 8.5x23x15 nm filled with the bulk liquid (dodcecane-DINP mixtures, or silicone oils), with periodic boundary conditions applied in all three directions (see Fig. 1). The liquid molecules were packed using Monte-Carlo algorithm. All initial configurations were built using the Scienomics MAPS package [46,47]. The system was then energy minimized using the steepest descent method, followed by the conjugate gradient method with a maximum number of iterations equal to 1000. Then, the simulation box was subjected to energy equilibration for 0.1 ns using the Langevin-thermostat in the NPT ensemble. Finally, production runs were launched for 0.25 ns in the isothermal-isochoric (NVT) ensemble to keep the system at a desired temperature of 298.15 K, and maintained by a Nose–Hoover thermostat [48,49].

3. Results and discussion

3.1. Effect of capillary bridges on suspension rheology

The addition of small amounts of a secondary liquid to particle suspensions may induce the formation of pendular secondary liquid bridges creating a percolating network to form pendular state capillary suspensions [1]. Fig. 2 (B) and (D) confirm this, showing pendular capillary bridges in a capillary suspension formed by adding a small amount of water to silica particles suspended in dodecane. The formation of capillary bridges drastically changes the rheological behavior, as already visually recognizable in Fig. 2 (A and C).

Fig. 3 shows the storage (G') and loss (G'') moduli of the regular (i.e., without the addition of a secondary liquid) and the capillary suspension as a function of shear strain. All other examined regular and capillary suspensions showed similar trends, and the results in Fig. 3 are taken from just one sample as an example to visualize the effect of the presence of liquid bridges. At low strain, the regular and capillary suspensions show constant storage and loss moduli, with G' surpassing G''. Hence, both systems show gel-like behavior. The addition of a small amount of water to the regular suspension results in a sharp increase in G', corresponding to a drastic strengthening of the particle network. The capillary suspension has a lower loss tangent $\tan\delta$ (G''/G') than the regular suspension in the linear viscoelastic region, indicating a more elastic-driven behavior. This difference originates in the different interaction types and strengths. Whereas the capillary suspension network is formed by strong interactions induced by pendular bridges between

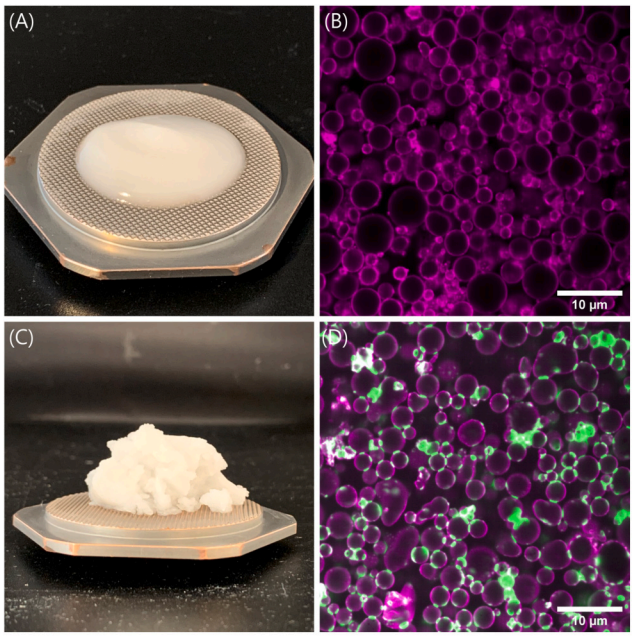

Fig. 2. Influence of secondary liquid addition on the visual appearance and network structure of suspensions. Photographs of regular (A) and capillary (C) suspensions prepared with 5 µm silica and dodecane as bulk liquid. CLSM images of regular (B) and capillary (D) suspensions prepared with 5 µm silica particles and dodecane as bulk liquid. Silica particles appear in magenta and water in green. Here, the solid fraction of silica is approx. 20% (v/v) mixed with 1.5% (v/v) of water.

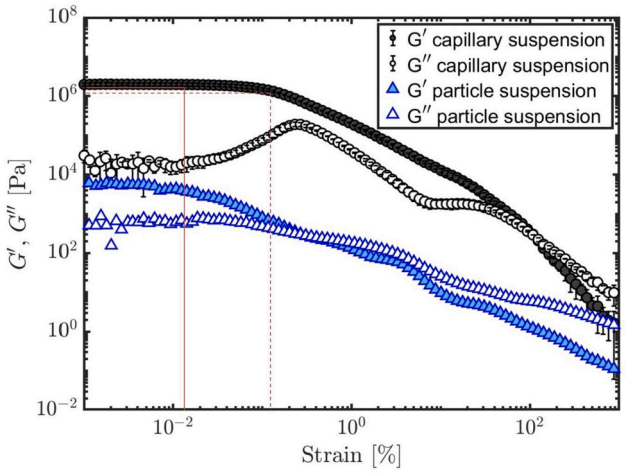

Fig. 3. Viscoelastic moduli (filled symbols, G'; open symbols, G'') as a function of strain amplitude obtained from amplitude sweeps for regular (blue triangles) and capillary (black circles) suspensions prepared with 5 µm silica particles and dodecane as bulk liquid. The continuous and dashed red lines schematically locate the maximum storage modulus (G'_{max}) and the yield strain (γ_y), respectively. Here, the solid fraction of silica is approx. 20% (v/v) mixed with 1.5% (v/v) of water. Shear strain was performed at a constant angular frequency ω of 1.6 Hz.

silica particles, only van der Waals interactions and hydrogen bonding between the silica particles induce gelation in the regular suspension [50].

With increasing strain, the moduli start to decrease, indicating the first structural changes within the network. In capillary suspensions, the first decrease in G' can be attributed to the stretching and breaking of small liquid bridges connecting the particles in the pendular state [51]. Concurrently, the G'' of the capillary suspensions shows a short-term in-

crease, known as a weak strain overshoot [52]. The weak overshoot may be explained by the partial breakdown and rearrangements at relatively low strain, causing increased collisions and hence viscous dissipation. With further increasing strain, the bridges are further stretched weakening the capillary bridge force, and the rupture of the bridges starts to dominate, indicating the start of a yielding process. The G'' eventually becomes larger than G' at the cross-over strain. This crossover suggests that the viscous properties dominate the elastic properties, and the material starts to behave liquid-like. As shown in Fig. 3, the capillary suspension starts to behave nonlinearly already at a strain of approximately 0.1%, while showing a cross-over at a higher strain than the regular suspension. This difference in the relative locations of the end of the linear viscoelastic region and cross-over emphasizes the dependence of the capillary bridge force on the particle separation, causing the initial weakening of the network. However, the capillary network exhibits resilience against fluidisation, related to fewer ruptures of the bridges [53]. Another characteristic of capillary suspensions is the dual yielding at large strain amplitudes common for systems where network build-up and network breakdown occur at similar time scales [54,55]. It has been suggested that the second yield point is caused by the advancing breakdown of fluidized clusters resulting from the first yielding [51].

3.2. Effect of the bulk liquid viscosity on the rheological behavior

By combining liquids with low and high viscosity, binary bulk liquids with a wide range of viscosities were prepared to investigate the effect of the bulk liquid viscosity on the rheological behavior of the resulting capillary suspensions. The experimentally measured viscosity of the bulk liquids mixtures is shown in Figures S4 and S5 of the SI Appendix. To quantify the observed changes in the gel strength, we use the maximum storage modulus ($G'_{\max}$) and yield stress (σ_y). $G'_{\max}$ is defined as the maximum value of the storage modulus G' within the linear viscoelastic region (LVR). It is determined as the average G' value until it decreases by 3% from its initial value, indicating the onset of nonlinear behavior [36,56] (see Fig. 3). The strain at which G' starts to decrease significantly from the LVR defines γ_y, and the corresponding stress at this point defines σ_y.

Fig. 4 shows information on the rheological behavior (A and B) of dodecane-DINP continuous capillary suspensions with variable bulk liquid viscosity prepared with silica particles and water as secondary liquid. Specifically, $G'_{\max}$ and σ_y are shown as a function of the viscosity ratio between the bridging and bulk liquid, defined as $\lambda = \eta_{\text{sec. liquid}}/\eta_{\text{bulk liquid}}$. A lower value for the viscosity ratio refers to a higher viscosity of the bulk liquid. This is represented for dodecane-DINP capillary suspensions prepared with two different sizes; 5 μm (black symbols) and 10 μm (open symbols) silica particles. The corresponding calculated capillary bridge forces (Equation (1)) are included as well at the bottom of Fig. 4 (B). In addition, photographs of the macroscopic structure of the gels are provided in Figure S6 of the SI appendix. The interfacial tension and the three-phase contact angle, which are used to calculate the capillary force, are shown in Figures S7 to S12 of the SI Appendix. With increasing viscosity ratio, i.e. decreasing bulk liquid viscosity, $G'_{\max}$ and σ_y increase, indicating an increasing gel strength. Both $G'_{\max}$ and σ_y show a similar trend of a relatively steep initial increase below a viscosity ratio of approximately 0.1 before exhibiting a plateau-like behavior. This may be unexpected, as a more viscous bulk phase would intuitively lead to more viscous suspensions. This apparent change in the gel strength-viscosity ratio relationship potentially indicates a transition point resembling the onset of a bulk liquid viscosity effect. The capillary bridge force shows a similar trend as a function of the viscosity ratio due to the changing dodecane-DINP ratio, possibly contributing to the decreasing gel strength with decreasing viscosity ratio. To verify that bulk liquid viscosity indeed has a large effect on the gel strength, we investigated a second system in which the bulk liquid viscosity was altered by a one-component continuous phase, silicone oil (see Figures S13 and S14 of the SI Appendix). The estimated capillary bridge force of the silicone oil continuous system is considerably constant within the examined range.

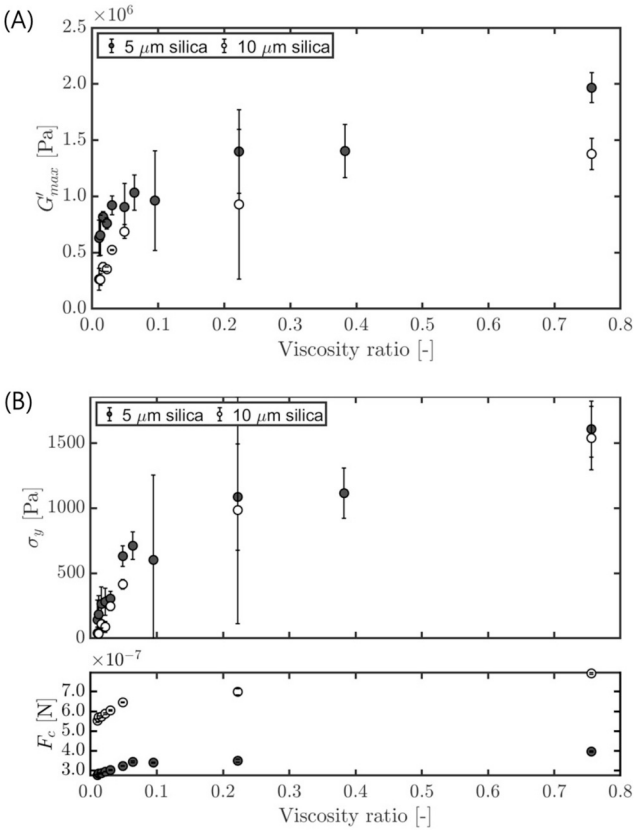

Fig. 4. Influence of the bulk liquid viscosity on the gel strength of capillary suspensions. Maximum storage modulus ($G'_{\max}$) (A), and yield stress (σ_y) (B) of dodecane-DINP continuous capillary suspensions prepared with either 5 μm (black symbols) or 10 μm (open symbols) silica particles as a function of the viscosity ratio $\eta_{\text{sec. liquid}}/\eta_{\text{bulk liquid}}$. Additionally, the estimated capillary bridge force (F_c) between the 5 μm (black symbols) or 10 μm (open symbols) silica particles as a function of the viscosity ratio $\eta_{\text{sec. liquid}}/\eta_{\text{bulk liquid}}$ is shown. In all cases, the solid fraction of silica particles is approx. 20% (v/v) mixed with 1.5% (v/v) of water. Shear strain was performed at a constant angular frequency ω of 1.6 Hz.

Fig. 5 displays $G'_{\max}$ of capillary suspensions as a function of the estimated capillary bridge force for 5 and 10 μm particles, and for silicone-oil and dodecane-DINP mixtures. In the case of dodecane-DINP mixtures, the increase of $G'_{\max}$ with the slight variation in F_c suggests a moderate dependence on capillary forces. The effect of increasing the particles size on $G'_{\max}$ is more pronounced. This aligns with the hypothesis that while capillary forces are important, other factors such as particle size and bulk liquid viscosity also influence the gel strength. The strength of gels made with silicone oil increases by orders of magnitude with minimal variation in capillary force. This supports the association between the bulk liquid viscosity and gel strength as the dominant effect. Given the similar rheological trends for silicone oil and dodecane-DINP, and due to visualization challenges with silicone oil where refractive index matching and fluorescence interference obscured the capillary bridges, we focused on CLSM imaging of dodecane-DINP systems.

Although the bulk liquid viscosity is not anticipated to directly impact the static capillary bridge force between two particles [57], we aim to understand its indirect effects which might explain the observed decrease in gel strength. Notably, gel strength depends not just on the capillary force of each liquid bridge, but also on the overall number of such bridges (see Equation (2)) [20]. As capillary suspensions are not in thermodynamic equilibrium but rather in a metastable state, the final

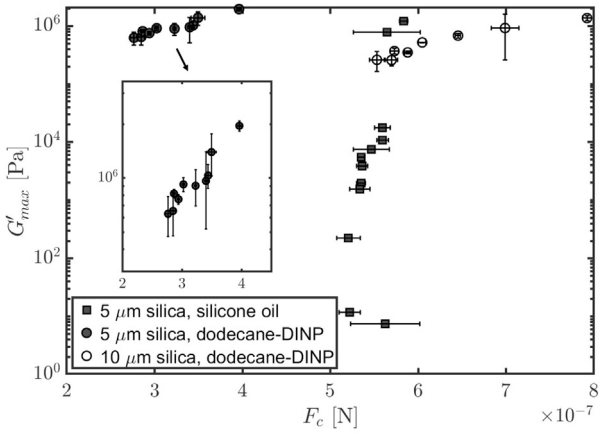

Fig. 5. Average G'_{max} of capillary suspensions as a function of the estimated capillary bridge force, for dodecane-DINP mixtures (circles symbols), and silicone oils (square symbols) for different particle sizes. The inset graph shows a zoomed-in region of 5 μm dodecane-DINP mixtures. In all cases, the solid fraction of silica particles is approx. 20% (v/v) mixed with 1.5% (v/v) of water. Shear strain was performed at a constant angular frequency ω of 1.6 Hz.

network structure is dependent on the mixing process during the preparation of capillary suspension [58]. Breaking the secondary liquid into tiny droplets during the mixing process is a well-recognized aspect and critical, as these droplets serve as building blocks for capillary bridges [12,20,31]. Thus, the mixing process ultimately impacts the strength of the capillary suspensions. It has been shown that the viscosity ratio has a large effect on the critical capillary number [28], thereby influencing the break-up of the droplet. It was shown that the smallest droplets are formed at viscosity ratios ranging from 0.1 to 1 while the droplet size increases to a large extent when the viscosity ratio is lower than 0.1. The breakup of dispersed droplets becomes increasingly difficult for viscosity ratios below 0.1 due to a very high viscosity of the continuous bulk viscosity, in which elongation and breakup of the dispersed droplets is inhibited. Based on the results of Grace [28], it is reasonable to argue that for higher bulk viscosities (with a viscosity ratio lower than 0.1), one expects larger but fewer secondary liquid droplets, i.e. fewer capillary bridges, and hence a weakening effect of the particle network. The hindered droplet breakup is consistent with the observed lower G' for our capillary suspension (Fig. 4), with decreasing viscosity ratio. It must be noted that the droplet breakup model by Grace [28] applies to mixing in the laminar flow regime, which is not fulfilled by the use of the dispersion mixer for the preparation of our capillary suspensions. Furthermore, the presence of particles increases the complexity of the droplet breakup during sample preparation [59].

Although the effect of the viscosity ratio by changing the bulk liquid on the strength of capillary suspension has not been discussed yet in literature, previous studies have reported the effect of changing the secondary bridging liquid viscosity using polyethylene oxide [12]. No significant change in the gel strength was observed with increasing secondary bridging liquid viscosity. The insignificance of the viscosity ratio was explained by the diffusion of secondary liquid driven by the energetic benefit of bridge formation [12]. Our results show that the viscosity of the bulk fluid is more relevant and has a much greater contribution to the behavior of capillary suspensions. We suspect that resistance to flow, increasing with the bulk liquid viscosity, contributes to the observed weakening of the capillary suspensions. To further understand the effect of the bulk liquid viscosity on the dynamics and break-up of capillary suspensions, numerical simulations are provided later in section 3.4.

We further note that the capillary suspensions prepared with 5 μm silica particles were stronger than the 10 μm samples across the examined bulk liquid viscosities, although a higher force would be expected for larger particles according to Equation (1). This reciprocal relationship between particle size and gel strength was previously reported in literature [13,19,60]. The lower gel strength indicates that the lower number of bridges between the particles due to the lower surface area contributes more to the final strength and yield stress than the force per bridge.

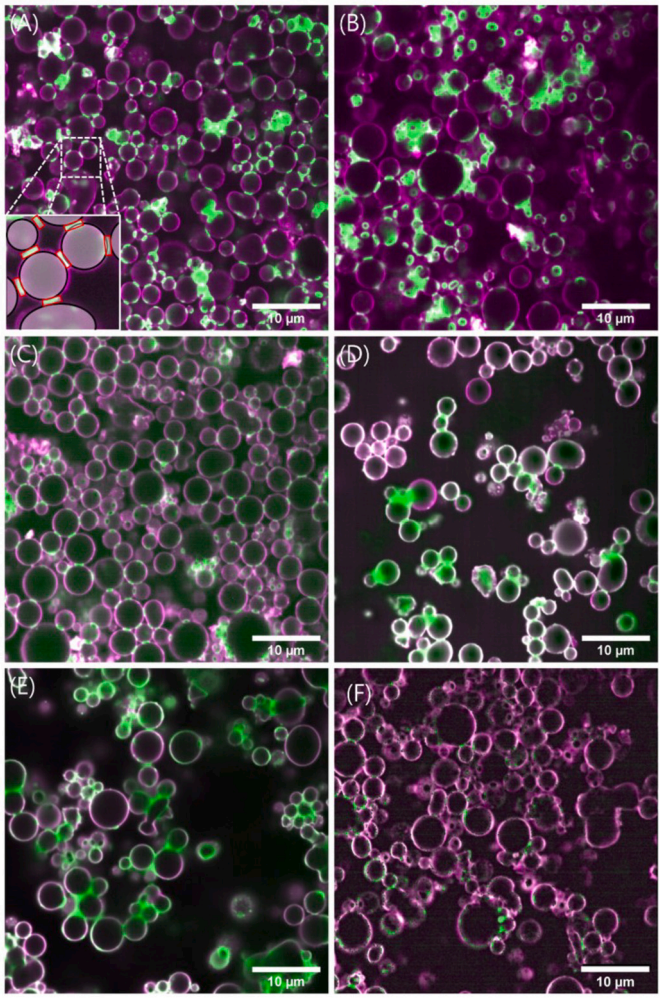

Fig. 6. CLSM images of dodecane-DINP continuous capillary suspensions prepared using 5 μm silica particles and bulk liquid viscosities of 1.32 mPas (A), 2.62 mPas (B), 4.51 mPas (C), 10.55 mPas (D), 45.03 (E), and 94.91 mPas (F). Silica particles appear in magenta, and water in green. The inset marks all pendular bridges (red rectangles) and particles (black circles) within the specified image section. In all cases, the solid fraction of silica particles is approx. 20% (v/v) mixed with 1.5% (v/v) of water.

Besides the effect of the bulk liquid viscosity on the gel strength, we investigated the impact on the yielding behavior. Figure S15 of the SI appendix shows the yield strain, γ_y, as a function of the viscosity ratio for dodecane-DINP capillary suspensions. Similarly to G' and σ_y (see Fig. 4), γ_y increases with increasing viscosity ratio, i.e. lower bulk liquid viscosity. In principle, the yielding of capillary suspensions is coupled to the stretching and, finally, rupture of the capillary bridges [16,31,51]. The decreasing γ_y suggests that the bridge elongation before rupture is reduced by increasing bulk liquid viscosity. The maximum bridge elongation before rupture is expected to increase with increasing bridge volumes [23,51]. Consequently, based on the droplet breakup discussion, we expect to see increasing γ_y with decreasing viscosity ratios. This contradiction implies the necessity of additional modes of action of the bulk liquid viscosity, which will be further elucidated in subsequent sections of this paper through the employment of numerical simulations.

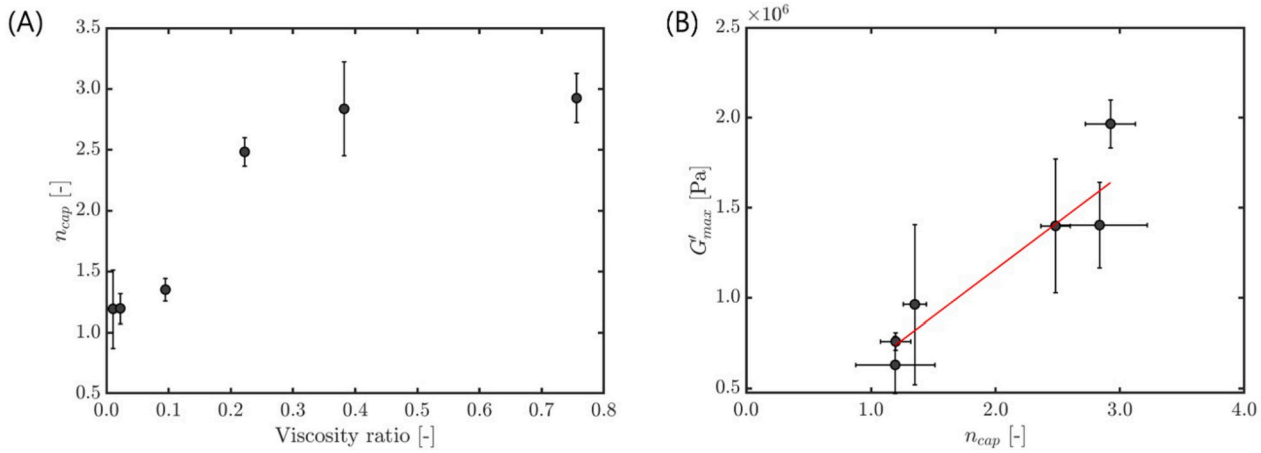

Fig. 7. (A) Average number of capillary bridges per particle (n_{cap}) as a function of the viscosity ratio $\eta_{\text{sec. liquid}}/\eta_{\text{bulk liquid}}$ of dodecane-DINP continuous capillary suspensions prepared with 5 μm silica particles. (B) Maximum storage modulus (G'_{max}) as a function of the average number of capillary bridges per particle of dodecane-DINP continuous capillary suspensions prepared with 5 μm silica particles. The red line shows the best linear fit accounting for confidence levels.

3.3. The effect of the bulk liquid viscosity on the network structure

To further understand the mechanistic effects of changing bulk liquid viscosity on the network structure, we visualized the network structure using confocal laser scanning microscopy (CLSM) micrographs. Fig. 6 shows CLSM images of capillary suspensions prepared with 5 μm silica particles, with varying dodecane-DINP ratios, used to alter the bulk liquid viscosity. The CLSM images are representative slices from the z-stacks of each sample. The overall particle volume is consistent across all samples, as indicated by the absence of visible syneresis or gel collapse (Figure S6 of the SI appendix). Within the examined bulk liquid viscosity range, a percolating network of silica particles (visible in magenta) connected by individual capillary secondary liquid bridges (visible in green) is present, confirming the pendular state. As the bulk liquid viscosity decreases, the particulate system appears to become homogeneous due to the formation of more liquid bridges.

To quantify the structural changes upon increasing bulk liquid viscosity, we adopted a simple approach of calculating the average number of bridges per particle from the acquired 2D CLSM images, n_{cap}, to characterize the interconnectivity within the network. The resulting average number of bridges per particle of selected dodecane-DINP continuous capillary suspensions prepared with 5 μm silica particles and variable bulk liquid viscosity are presented in Fig. 7 (A). A decrease in the average number of bridges per particle with decreasing viscosity ratio, i.e. increasing bulk liquid viscosity, is shown. This is consistent with few connections between particles as a result of fewer, and most likely larger, secondary liquid droplets. The data shows a relation between the bulk liquid viscosity, or the viscosity ratio, and the interconnectivity of the percolating network. While this suggests a trend, additional studies may be needed to fully confirm this relationship.

Moreover, when we plot the maximum storage modulus G'_{max} against n_{cap} (see Fig. 7 (B)), we see a positive trend between the gel strength and the degree of microscopic interconnectivity. Consequently, the observed trends in the macroscopic rheological behavior of the capillary suspensions can therefore be related to an indirect effect of the bulk liquid viscosity on the microscopic interconnectivity of the capillary suspension network structure. To gain deeper insights into the underlying mechanisms leading to decreased interconnectivity, we further explore the system using numerical simulations.

3.4. Numerical simulations

In initial numerical experiments, we explore the capacity of the capillary force in a liquid bridge to spontaneously bring together two particles. First, we examine this phenomenon in the presence of air, and subsequently, we assess its behavior in the presence of various bulk liquids with distinct viscosities. In Fig. 8 (A), we show snapshots of an MD simulation of the two particles, separated by a distance of 5 nm, connected by a water liquid bridge in the absence of a bulk liquid. At the simulation time $t = 0$ ps, the liquid bridge has cylindrical shape, representing the starting conditions of the system before any relaxation or energy minimization has occurred. As the MD simulation proceeds, the surface tension causes a thin film of water molecules to adhere to the particles and a concave meniscus starts to form. As the particles spontaneously move closer together, the adhesive intermolecular

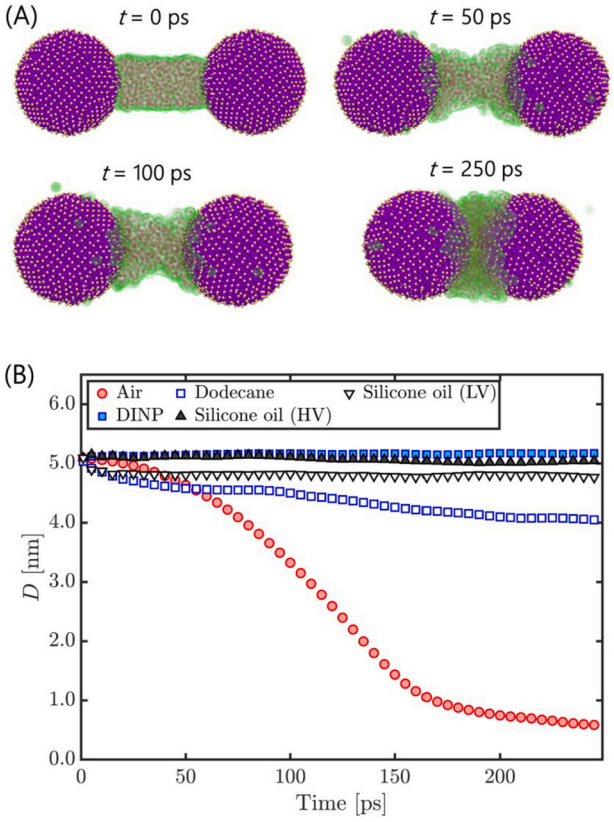

Fig. 8. (A) Time snapshots of a molecular dynamics simulation of two silica particles (in magenta) connected by a water liquid bridge (in green) surrounded by air, and (B) Distance between the two particles as a function of simulation time. LV: low viscous and HV: high viscous.

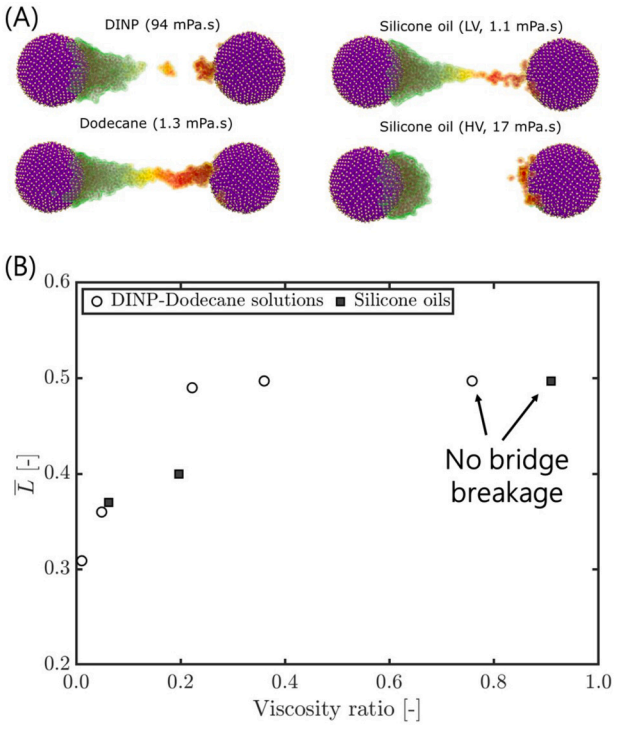

Fig. 9. (A) MD simulation snapshots of the finals simulation step of two silica particles (in magenta) connected by a water liquid bridge surrounded by various bulk liquids. The bulk liquids are transparent, and (B) Breakage distance ratio, $\overline{L}$, as a function of the viscosity ratio, $\eta_{\text{sec. liquid}}/\eta_{\text{bulk liquid}}$, for various bulk liquids. LV: low viscous and HV: high viscous.

forces between the particles and the fluid increase, pulling the particles together. The bridge becomes more pronounced, increasing the contact area between the particles and the fluid, which also increases the capillary force. This process continues until the particles are in close proximity from each other. This can also be seen by the curve of the red circles in Fig. 8 (B), showing the distance between the two particles as a function of simulation time. When using dodecane as a bulk liquid instead of air (open squares), there is a slower spontaneous pulling of the particles and a concave bridge forms (see also the video provided in the SI Video Appendix) during the examined simulation time. This is due to the lower interfacial tension between the water and dodecane compared to air. No spontaneous pulling happens between the particles for silicone oil systems mainly due to their low interfacial tension with water. In the case of DINP, a liquid that is more viscous than dodecane, the simulation shows that the inter-particle distance remains almost constant, and thus there is no occurrence of spontaneous pulling between the particles. This behavior can be attributed to both the lower DINP-water interfacial tension compared to dodecane-water and the high viscosity of DINP. We postulate that the high viscosity of DINP can affect the stability of the liquid bridges and increases the resistance to flow. Consequently, it becomes more challenging for the liquid bridge to form and maintain its shape. Additionally, the drag force on the particles increases for high viscous liquids, making it difficult for the capillary force to move the particles close to each other. As a result, as the viscosity of the encompassing liquid rises, the capacity of the capillary bridges to uphold the capillary network deteriorates, providing a plausible explanation for the feeble gel structures observed experimentally when utilizing high-viscosity bulk liquids. To further investigate this deduction, we proceed to conduct a second numerical experiment on the dynamics of capillary bridges break-up.

In this ensuing numerical experiment, the two particles were initially placed at a distance of 1 nm from each other, and we ran a molecular dynamics simulation in the NVT ensemble for 0.5 ns to let the liquid bridge molecules distribute around the particles. Then, the right-sided particle was pulled away at a velocity of 50 nm/ns. The video in the SI Video Appendix shows the pulling experiment over time. As the particle is pulled away, water molecules at the center of the bridge are pulled towards the left side of the bridge where the pulling stress is the lowest. The liquid bridge stretches and elongate and the radius of the curvature of the bridge increases. This stretching causes the cohesive forces between the water molecules to weaken. As the bridge thins out, the number of water molecules in contact with each particle decreases and the cohesive forces due to hydrogen bonds between the water molecules and the particles will also decrease. This progressively increases the surface area of the bridge in contact with the bulk liquid in detriment of that in contact with particles, until the bridge breaks-up.

Fig. 9 (A) shows snapshots of the final simulation step for various bulk liquids used. The bulk liquid is transparent and only the silica particles (in magenta) and the water bridge are shown. The gradient color represents the velocity of the water molecules within the liquid bridge. In Fig. 9 (B), we plot the breakage distance ratio $\overline{L} = D/L$, as a function of the viscosity ratio, where D is the distance between the particles and L the length of the simulation box. When using bulk liquids with high viscosity (highly viscous silicone oil and pure DINP), the break-up point occurs at lower distances, confirming that bridges are more difficult to elongate and stretch with increasing bulk liquid viscosity. This aligns with the research of Stone [61,62], who investigated the breakup of a liquid drop driven by the movement of an immiscible viscous suspending fluid, and showed that higher viscosity ratios tend to hinder the breakup process and favor stretching. In the case of low viscous bulk liquids (with viscosity ratio above 0.4 such as pure dodecane), as the right particle is pulled towards the simulation box boundary, the bridge undergoes continuous stretching. Although their study focused on suspended droplets, the differences in breakup behavior across viscosity ratios observed by Tjahjadi and Ottino [63] align with trends seen in our capillary bridge experiments. They investigated the stretching and breakup of drops freely suspended in a viscous fluid. Drops in low-viscosity-ratio systems extended relatively little before breaking, whereas droplets in high-viscosity-ratio systems stretched substantially before breaking. Jiang et al. [64] examined the effect of viscosity ratio on the local pinch-off mechanism of liquid drops in viscous fluids. They showed that the viscosity ratio indeed affects the drop pinch-off dynamics as well as interface deformation, where liquid bridges exhibit more tendency to stretch, and break after a longer time in low-viscosity bulk liquids.

As the viscosity of the bulk liquid increases, the resistance to flow also increases as the surrounding viscous liquid resists the movement of the water molecules in the liquid bridge, making it harder for the liquid bridge to thin out and stretch. This explains the reduction of the bridge elongation before rupture at high viscous bulk liquid (i.e. low viscosity ratio), as indicated by the low yield strain, γ_y, observed in Figure S15 of the SI appendix. Consequently, such rapid breakup could potentially lead to a reduced interconnectivity in capillary suspensions, which results in a weaker gel. Similarly to G'_{max} and σ_y, we observe a sharp increase in the breakup distance, $\overline{L}$, at a viscosity ratio of approximately 0.1, which further supports that there is a transition point for the effect of bulk liquid viscosity.

Fig. 10 depicts the total count of hydrogen bonds, H_{bonds}, formed by water molecules immediately prior to bridge breakage, as a function of the viscosity ratio. As the viscosity ratio increases (i.e. viscosity of the bulk liquid decreases), the total number of hydrogen bonds at the cusp of liquid bridge breakage increases, indicating that high bulk liquid viscosity reduces the ability of water molecules to dynamically form hydrogen bonds. Additionally, in the supplementary file's Figure S18, we present the total number of hydrogen bonds as a function of simulation time for the various bulk liquids used in this study. The results show that H_{bonds} reaches a minimum as the liquid bridges elongates. Subsequently, upon liquid bridge breakage, H_{bonds} begins to rise as water molecules re-form bonds and spread on the silica particles. This supports

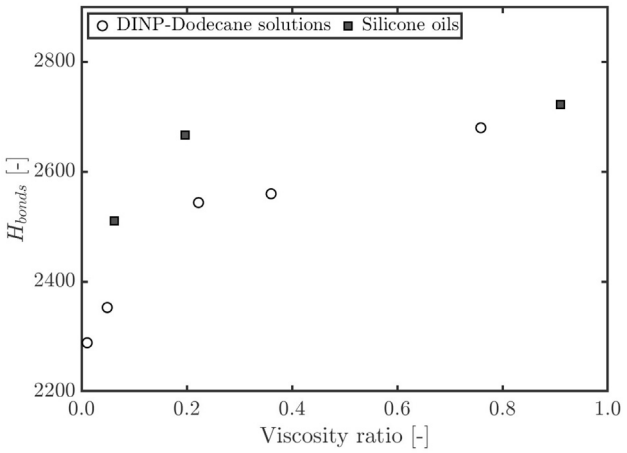

Fig. 10. Total number of hydrogen bonds, H_{bonds}, formed between the water molecules at the cusp of liquid breakage as a function of the viscosity ratio, $\eta_{\text{sec. liquid}}/\eta_{\text{bulk liquid}}$, for various bulk liquids.

the hypothesis that high bulk liquid viscosity reduces water molecules mobility, potentially leading to fewer hydrogen bonds formation, which in turn impedes the liquid bridge thinning and contributes to its premature breakage during pulling.

4. Conclusions

Capillary suspensions are ternary liquid-liquid-solid systems marked by liquid bridges that link suspended particles. These systems hold promise for the development of novel stimuli-responsive materials [5], 3D printing pastes [9,10], and healthier food products [11,12]. Through experiments and numerical simulations, we provide novel insights into the effects of the bulk liquid viscosity on the rheological and structural properties of capillary suspensions.

Our experiments show that capillary suspensions prepared with 5 μm silica particles exhibit higher gel strength compared to those with 10 μm particles, irrespective of the bulk liquid viscosity. Previous studies found no significant effect on gel strength due variations in secondary bridging liquid viscosity [12,31]. This was attributed to the energetically favored bridge formation through secondary liquid diffusion. Contrarily, our results show that the viscosity of the bulk fluid is more relevant and has a greater impact on capillary suspension behavior, with increased viscosity reducing the suspension's strength. This was attributed to alterations in microstructural configuration, characterized by a decrease in the average number of bridges per particle in weak gels. This indicates a link between bulk liquid viscosity (or viscosity ratio) and the interconnectivity of the percolating network. Additionally, increasing bulk liquid viscosity reduces the bridge elongation before fracture, as indicated by the decreasing yield strain. This reduction suggests that highly viscous bulk liquids impede the elongation of capillary bridges, potentially leading to diminished interconnectivity and weaker gels. We explored this mechanism further using molecular dynamics simulations, which showed that the breakup of liquid bridges occurs at shorter distances when highly viscous bulk liquids are present. This behavior stems from the resistance imposed by the surrounding viscous medium, restricting water molecule mobility within the liquid bridge. As a result, hydrogen bond reformation is diminished, leading to decreased water liquid bridge elongation and thinning during particle separation. Another insight from this work is the identification of a viscosity ratio threshold (≈ 0.1), beyond which the effect of bulk liquid viscosity on gel strength, yield stress, and liquid bridge breakup distance becomes markedly pronounced.

Using the viscosity of the bulk liquid to control the micro-structure and rheological behavior of capillary suspensions opens up possibilities for designing new materials with tailored properties. To enhance comprehension of how bulk liquid viscosity influences capillary suspension structures, exploring the impact of external heating during preparation is worthwhile. Additionally, optical tweezers could be used to dynamically investigate the effect of the bulk liquid viscosity on the strength and breakup distance of individual pendular bridges.

CRediT authorship contribution statement

Christoph Haessig: Writing – review & editing, Writing – original draft, Visualization, Validation, Methodology, Investigation, Formal analysis, Data curation. **Jasper Landman:** Writing – review & editing, Methodology, Conceptualization. **Elke Scholten:** Writing – review & editing, Supervision, Resources, Project administration, Methodology, Funding acquisition, Conceptualization. **Ahmed Jarray:** Writing – review & editing, Writing – original draft, Visualization, Supervision, Software, Resources, Project administration, Methodology, Investigation, Funding acquisition, Formal analysis, Data curation, Conceptualization.

Declaration of competing interest

The authors declare the following financial interests/personal relationships which may be considered as potential competing interests: Ahmed Jarray reports financial support was provided by Dutch Research Council. If there are other authors, they declare that they have no known competing financial interests or personal relationships that could have appeared to influence the work reported in this paper.

Data availability

Data will be made available on request.

Acknowledgements

This work was financially supported by the Netherlands Organisation for Scientific Research (NWO-KLEIN, OCENW.KLEIN.303). We thank Stefan Luding and Wouter K. den Otter for their help and suggestions.

Appendix A. Supplementary material

Supplementary material related to this article can be found online at https://doi.org/10.1016/j.jcis.2024.09.021.

References

[1] Erin Koos, Norbert Willenbacher, Capillary forces in suspension rheology, Science 331 (6019) (2011) 897–900.
[2] Jens Dittmann, Erin Koos, Norbert Willenbacher, Ceramic capillary suspensions: novel processing route for macroporous ceramic materials, J. Am. Ceram. Soc. 96 (2) (2013) 391–397.
[3] Jens Dittmann, Norbert Willenbacher, Micro structural investigations and mechanical properties of macro porous ceramic materials from capillary suspensions, J. Am. Ceram. Soc. 97 (12) (2014) 3787–3792.
[4] Johannes Maurath, Jens Dittmann, Niko Schultz, Norbert Willenbacher, Fabrication of highly porous glass filters using capillary suspension processing, Sep. Purif. Technol. 149 (2015) 470–478.
[5] Anupam A.K. Das, Timothy S. Dunstan, Simeon D. Stoyanov, Pierre Starck, Vesselin N. Paunov, Thermally responsive capillary suspensions, ACS Appl. Mater. Interfaces 9 (50) (2017) 44152–44160.
[6] Monica Schneider, Erin Koos, Norbert Willenbacher, Highly conductive, printable pastes from capillary suspensions, Sci. Rep. 6 (2016) 31367.
[7] Monica Schneider, Johannes Maurath, Steffen B. Fischer, Moritz Weiß, Norbert Willenbacher, Erin Koos, Suppressing crack formation in particulate systems by utilizing capillary forces, ACS Appl. Mater. Interfaces 9 (12) (2017) 11095–11105.
[8] Boris Bitsch, Jens Dittmann, Marcel Schmitt, Philip Scharfer, Wilhelm Schabel, Norbert Willenbacher, A novel slurry concept for the fabrication of lithium-ion battery electrodes with beneficial properties, J. Power Sources 265 (2014) 81–90.
[9] Johannes Maurath, Norbert Willenbacher, 3d printing of open-porous cellular ceramics with high specific strength, J. Eur. Ceram. Soc. 37 (15) (2017) 4833–4842.
[10] Sangchul Roh, Dishit P. Parekh, Bhuvnesh Bharti, Simeon D. Stoyanov, Orlin D. Velev, 3d printing by multiphase silicone/water capillary inks, Adv. Mater. 29 (30) (2017) 1701554.

[11] Susanne Wollgarten, Ceren Yuce, Erin Koos, Norbert Willenbacher, Tailoring flow behavior and texture of water based cocoa suspensions, Food Hydrocoll. 52 (2016) 167–174.
[12] Susanne Hoffmann, Erin Koos, Norbert Willenbacher, Using capillary bridges to tune stability and flow behavior of food suspensions, Food Hydrocoll. 40 (2014) 44–52.
[13] Erin Koos, Capillary suspensions: particle networks formed through the capillary force, Curr. Opin. Colloid Interface Sci. 19 (6) (2014) 575–584.
[14] Erin Koos, Norbert Willenbacher, Particle configurations and gelation in capillary suspensions, Soft Matter 8 (14) (2012) 3988–3994.
[15] Frank Bossler, Erin Koos, Structure of particle networks in capillary suspensions with wetting and nonwetting fluids, Langmuir 32 (6) (2016) 1489–1501.
[16] Trystan Domenech, Sachin S. Velankar, On the rheology of pendular gels and morphological developments in paste-like ternary systems based on capillary attraction, Soft Matter 11 (8) (2015) 1500–1516.
[17] J.P.K. Seville, C.D. Willett, P.C. Knight, Interparticle forces in fluidisation: a review, Powder Technol. 113 (3) (2000) 261–268.
[18] Jens Allard, Sanne Burgers, Miriam Candelaria Rodríguez González, Yanshen Zhu, Steven De Feyter, Erin Koos, Effects of particle roughness on the rheology and structure of capillary suspensions, Colloids Surf. A, Physicochem. Eng. Asp. 648 (2022) 129224.
[19] E. Koos, J. Johannsmeier, L. Schwebler, N. Willenbacher, Tuning suspension rheology using capillary forces, Soft Matter 8 (24) (2012) 6620–6628.
[20] Frank Bossler, Lydia Weyrauch, Robert Schmidt, Erin Koos, Influence of mixing conditions on the rheological properties and structure of capillary suspensions, Colloids Surf. A, Physicochem. Eng. Asp. 518 (2017) 85–97.
[21] Hans-Jürgen Butt, Michael Kappl, Normal capillary forces, Adv. Colloid Interface Sci. 146 (1–2) (2009) 48–60.
[22] Stephan Herminghaus, Dynamics of wet granular matter, Adv. Phys. 54 (3) (2005) 221–261.
[23] Christopher D. Willett, Michael J. Adams, Simon A. Johnson, Jonathan P.K. Seville, Capillary bridges between two spherical bodies, Langmuir 16 (24) (2000) 9396–9405.
[24] S. Strauch, S. Herminghaus, Wet granular matter: a truly complex fluid, Soft Matter 8 (32) (2012) 8271–8280.
[25] David Megias-Alguacil, Ludwig J. Gauckler, Capillary forces between two solid spheres linked by a concave liquid bridge: regions of existence and forces mapping, AIChE J. 55 (5) (2009) 1103–1109.
[26] W. Pietsch, Hans Rumpf, Haftkraft, Kapillardruck, Flüssigkeitsvolumen und Grenzwinkel einer Flüssigkeitsbrücke zwischen zwei Kugeln, Chem. Ing. Tech. 39 (15) (1967) 885–893.
[27] T. Domenech, S. Velankar, Capillary-driven percolating networks in ternary blends of immiscible polymers and silica particles, Rheol. Acta 53 (8) (2014) 593–605.
[28] H.P. Grace, Dispersion phenomena in high viscosity immiscible fluid systems and application of static mixers as dispersion devices in such systems, Chem. Eng. Commun. 14 (3–6) (1982) 225–277.
[29] Jeewon Yang, Hyun-su Park, Jieun Kim, Jihye Mok, Taeyeon Kim, Eun-kyung Shin, Chaesu Kwak, Sehyeong Lim, Chae Bin Kim, Jong-Sung Park, et al., Yield stress enhancement of a ternary colloidal suspension via the addition of minute amounts of sodium alginate to the interparticle capillary bridges, Langmuir 36 (32) (2020) 9424–9435.
[30] Amit Ahuja, Chaiwut Gamonpilas, Rheology of thermo-gelling capillary suspensions, Colloid Polym. Sci. 299 (1) (2021) 165–176.
[31] Sebastian Bindgen, Jens Allard, Erin Koos, The behavior of capillary suspensions at diverse length scales: from single capillary bridges to bulk, Curr. Opin. Colloid Interface Sci. 58 (2022) 101557.
[32] Diana Lievano, Sachin Velankar, Joseph J. McCarthy, The rupture force of liquid bridges in two and three particle systems, Powder Technol. 313 (2017) 18–26.
[33] Bryan J. Ennis, Jianlan Li, Pfeffer Robert, et al., The influence of viscosity on the strength of an axially strained pendular liquid bridge, Chem. Eng. Sci. 45 (10) (1990) 3071–3088.
[34] Zhang Shi, Yi Zhang, Mingchao Liu, Dorian A.H. Hanaor, Yixiang Gan, Dynamic contact angle hysteresis in liquid bridges, Colloids Surf. A, Physicochem. Eng. Asp. 555 (2018) 365–371.
[35] Xiangqi Li, Dengfei Wang, Fenglei Huang, Ziqi Cai, Zhengming Gao, Stretching and rupture of a viscous liquid bridge between two spherical particles, Asia-Pac. J. Chem. Eng. 16 (1) (2021) e2579.
[36] Zipeng Liu, Huan Chen, Bo Zheng, Fengwei Xie, Ling Chen, Understanding the structure and rheological properties of potato starch induced by hot-extrusion 3d printing, Food Hydrocoll. 105 (2020) 105812.
[37] Suresh G. Sutariya, Prafulla Salunke, Effect of hyaluronic acid on milk properties: rheology, protein stability, acid and rennet gelation properties, Food Hydrocoll. 131 (2022) 107740.
[38] J. Schindelin, I. Arganda-Carreras, E. Frise, V. Kaynig, M. Longair, T. Pietzsch, S. Preibisch, C. Rueden, S. Saalfeld, B. Schmid, J.Y. Tinevez, D.J. White, V. Hartenstein, K. Eliceiri, P. Tomancak, A. Cardona, Fiji: an open-source platform for biological-image analysis, Nat. Methods 9 (7) (2012) 676–682.
[39] Sabine Leroch, Martin Wendland, Influence of capillary bridge formation onto the silica nanoparticle interaction studied by grand canonical Monte Carlo simulations, Langmuir 29 (40) (2013) 12410–12420.
[40] Jacob N. Israelachvili, Intermolecular and Surface Forces, Academic Press, 2011.
[41] Ahmed Jarray, Annika Feichtinger, Elke Scholten, Linking intermolecular interactions and rheological behaviour in capillary suspensions, J. Colloid Interface Sci. 627 (2022) 415–426.
[42] Steve Plimpton, Fast parallel algorithms for short-range molecular dynamics, J. Comput. Phys. 117 (1) (1995) 1–19.
[43] Huai Sun, Zhao Jin, Chunwei Yang, Reinier L.C. Akkermans, Struan H. Robertson, Neil A. Spenley, Simon Miller, Stephen M. Todd, Compass ii: extended coverage for polymer and drug-like molecule databases, J. Mol. Model. 22 (2016) 1–10.
[44] Frederik Tielens, Christel Gervais, Jean François Lambert, Francesco Mauri, Dominique Costa, Ab initio study of the hydroxylated surface of amorphous silica: a representative model, Chem. Mater. 20 (10) (2008) 3336–3344.
[45] Daniël P. Faasen, Ahmed Jarray, Harold J.W. Zandvliet, E. Stefan Kooij, Wojciech Kwiecinski, Hansen solubility parameters obtained via molecular dynamics simulations as a route to predict siloxane surfactant adsorption, J. Colloid Interface Sci. 575 (2020) 326–336.
[46] D.N. Theodorou, U.W. Suter, Detailed molecular structure of a vinyl polymer glass, Macromolecules 18 (7) (1985) 1467–1478.
[47] Scienomics, Maps platform 4.2, http://www.scienomics.com/, March 2019.
[48] Shuichi Nosé, A unified formulation of the constant temperature molecular dynamics methods, J. Chem. Phys. 81 (1) (1984) 511–519.
[49] William G. Hoover, Canonical dynamics: equilibrium phase-space distributions, Phys. Rev. A 31 (3) (1985) 1695.
[50] Srinivasa R. Raghavan, Saad A. Khan, Shear-thickening response of fumed silica suspensions under steady and oscillatory shear, J. Colloid Interface Sci. 185 (1) (1997) 57–67.
[51] A. Ahuja, C. Gamonpilas, Dual yielding in capillary suspensions, Rheol. Acta 56 (10) (2017) 801–810.
[52] Gavin J. Donley, Piyush K. Singh, Abhishek Shetty, Simon A. Rogers, Elucidating the g" overshoot in soft materials with a yield transition via a time-resolved experimental strain decomposition, Proc. Natl. Acad. Sci. 117 (36) (2020) 21945–21952.
[53] Erin Koos, Wolfgang Kannowade, Norbert Willenbacher, Restructuring and aging in a capillary suspension, Rheol. Acta 53 (12) (2014) 947–957.
[54] Amit Ahuja, Andrei Potanin, Yogesh M. Joshi, Two step yielding in soft materials, Adv. Colloid Interface Sci. 282 (2020) 102179.
[55] Huagui Zhang, Kai Yu, Olivier J. Cayre, David Harbottle, Interfacial particle dynamics: one and two step yielding in colloidal glass, Langmuir 32 (50) (2016) 13472–13481.
[56] Thomas G. Mezger, et al., The Rheology Handbook, vol. 10, Vincentz Network, Hannover, Germany, 2012.
[57] H. Schubert, Capillary forces-modeling and application in particulate technology, Powder Technol. 37 (1) (1984) 105–116.
[58] Sachin S. Velankar, A non-equilibrium state diagram for liquid/fluid/particle mixtures, Soft Matter 11 (43) (2015) 8393–8403.
[59] Sukhvinder Kaur, L. Gary Leal, Drop deformation and break-up in concentrated suspensions, J. Rheol. 54 (5) (2010) 981–1008.
[60] Jonathan McCulfor, Paul Himes, Mark R. Anklam, The effects of capillary forces on the flow properties of glass particle suspensions in mineral oil, AIChE J. 57 (9) (2011) 2334–2340.
[61] Howard A. Stone, Dynamics of drop deformation and breakup in viscous fluids, Annu. Rev. Fluid Mech. 26 (1) (1994) 65–102.
[62] Howard A. Stone, B.J. Bentley, L.G. Leal, An experimental study of transient effects in the breakup of viscous drops, J. Fluid Mech. 173 (1986) 131–158.
[63] M. Tjahjadi, J.M. Ottino, Stretching and breakup of droplets in chaotic flows, J. Fluid Mech. 232 (1991) 191–219.
[64] Xiaofeng Jiang, Enle Xu, Xianliang Meng, Huai Z. Li, The effect of viscosity ratio on drop pinch-off dynamics in two-fluid flow, J. Ind. Eng. Chem. 91 (2020) 347–354.